

Monte Carlo Simulation of Shielding to Reduce Cosmic Radiation Damage to Semiconductors Loaded on Air Freighter Considering the Position of ULDs

Juhuk Lee, Heon Yong Jeong, Hyun Nam Kim, and Sung Oh Cho *
Department of Nuclear and Quantum Engineering, KAIST, Daejeon
*Corresponding author: socho@kaist.ac.kr

1. Introduction

Cosmic radiation, highly energetic particles from outer space, interacts with the atmosphere and cause a cascade of secondary cosmic radiation-induced-particles [1, 2]. At the flight altitude of 10~15 km, the particles most responsible for delivering high dose to electronic devices are neutrons and protons [3, 4]. It is generally stated that failure of the electronic devices from single event upsets can occur when energetic particles strike the devices during operation. However, the advancement in fabrication technology in recent years allows for smaller feature sizes in integrated circuits, which can lead to unexpected internal failures even when the devices are in off-state [5, 6]. This failure arises from the fact that energy deposition characteristics of protons and neutrons with energy corresponding to that at the flight altitude induce nuclear reactions in silicon. The reactions take place in the immediate vicinity of vulnerable components such as the gate oxide that ultimately can lead to the breakdown of semiconductors.

Due to high demand of memory semiconductors coupled with there being a limited number of vendors of the product, long flight to transport semiconductors is very common. Nonetheless, with the current packaging procedure, the memory semiconductors face high possibility of malfunctioning due to experiencing radiation-induced damages during air transport. The semiconductors are generally transported in Unit Load Devices (ULDs) that are regularly made of aluminum alloy. Aluminum is primarily used due to its remarkable mechanical properties relative to its low density; however, the material is not adequate for effectively shielding against neutrons and protons. Materials with high atomic numbers, such as iron and lead, are suitable for stopping protons while materials with low atomic numbers, such as polyethylene, are suitable for stopping neutrons. With all this in consideration, it is important to reinforce the current aluminum ULDs in a way that balances maximizing radiation shielding with minimizing weight. Also, the effect of fuel tank and engine of air freighter were considered to evaluate the proton and neutron spectra at each position of ULDs.

In this study, Monte Carlo simulations were performed to determine the optimal material and structure of the reinforcement within a ULD container for minimizing the number of neutrons and protons reaching the contents inside. In addition, the geometry of air freighter was modeled and the proton and neutron

spectra at each position of ULD containers inside air freighter were calculated.

2. Methods

MCNP 6.2 radiation transport code was used to calculate the interaction of cosmic radiation and the specification of generated protons and neutrons.

2.1. Cosmic radiation induced particles

To determine the energy spectra of protons and neutrons by incident angle at the flight altitude, the atmospheric model, modeled after those used in previous studies, was utilized [1, 2]. The atmosphere was designed to be a cuboid with a height of 65 km and a length and a depth of 50 km. The walls of the system were set to reflect to produce an infinite geometry; any particle striking a reflecting surface is reflected back into the system, preserving the number of particles in the model. The cuboid was divided to account for the changes in atmospheric density and humidity. The cosmic radiation generated at the top of the atmosphere and directed downwrad was composed of protons, alphas, and some heavy ions, such as nitrogen, silicon, and iron nuclei. The geographical coordinates were set to 23 S, 45W and the date was set to 01 March 2015. From these parameters, rigidity cut-off of 9.6 GV and solar modulation of 70 MV were obtained and were used to simulate cosmic radiation. The neutrons and protons reaching the flight altitude of 12.5 km were assessed for different solar incidence angles, varied in intervals of 15°, using the F1 type tally. The recorded energies and angles of the particles at the flight altitude were used to simulate the neutrons and protons reaching the container.

2.2. The modeling of container

The container geometry used for the calculation was modeled after the M-1 type ULD container shipped in the aircraft fuselage (Fig. 1(a)). The M-1 container is mainly composed of aluminum and is 3 mm thick on all sides. The model used for a simplified aircraft was a 5 mm thick aluminum cylinder that was only 30 m long to improve calculation efficiency. In order to simulate an infinite environment using the cube geometry, four lateral surfaces of the cube were set to be reflective. Fig. 1(b) shows the layout of the cube geometry, the radiation source, the reflective walls and the container

inside the aircraft fuselage. The top and bottom surfaces of the cube generate neutrons and protons with energies and angles determined previously for the flight altitude.

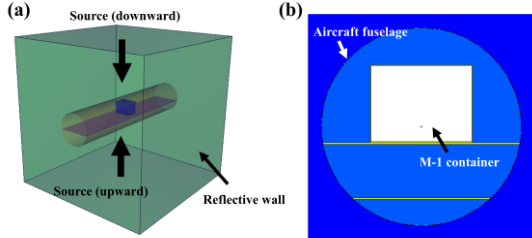


Figure 1. (a) 2D view and (b) 3D view of simulation geometry

2.3. The modeling of air freighter

The air freighter and the containers inside air freighter were modeled to evaluate energy information of protons and neutrons depending on the position of containers (Fig. 2). The CAD blueprint of Boeing 777F from the official website of the Boeing Company were referred for to model the geometry of fuselage including fuel tanks and engines. All the outer walls of the air freighter including wings were 5 mm thick aluminum loaded with 13 M-1 containers on the main deck and 16 LD3 containers on the low deck. The fuel tanks consisting of carbon, hydrogen, and sulfur, were located inside the two main wings and center of the low deck. The two engines were composed of titanium, aluminum, and iron and located below the two main wings. These engines referred to GE90 of General Electronic with the weight of 8760 kg. As the modeling in chapter 2.3, the neutrons and protons generated from top and bottom surface.

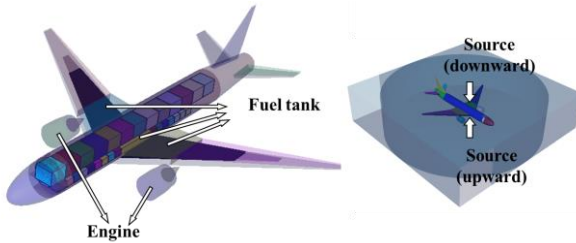


Figure 2. The modeling of air freighter and containers

3. Results

3.1. Cosmic radiation-induced neutrons and protons at the flight altitude

Fig. 3 shows the calculated energy spectra and angular distributions of protons and neutrons at the flight altitude of 12.5 km. The fluence value indicates the number of particles reaching the surface tally per generated source particle. Fig. 3(a) and (b) represent the energy spectra of neutrons and protons, respectively, entering at various angles. The angles were considered in intervals of 15° from 0° to 180° relative to the

negative vertical axis. Cosmic radiation-induced neutrons are generally divided into subgroups based on energy: thermal (under 0.55 eV), epithermal (0.55 eV ~ 0.1 MeV), evaporation (0.1 ~ 20 MeV), and cascade (above 20 MeV). In this study, the thermal and epithermal groups were merged (< 0.1 MeV), and neutrons with energy greater than 100 MeV within the cascade group were plotted separately to address the capability of shielding from high energy particles. Fig. 3(a) indicates isotropic distribution of neutrons that possess energy of less than 20 MeV, while for neutrons in the cascade group, it suggests the prominence of downwards pointing particles. These differing tendencies exhibited by the energy groups are well depicted in Fig. 3(c). Meanwhile, protons were classified into low (<100 MeV) and high energy (>100 MeV) groups. Fig. 3(b) and (d) indicate that at the flight altitude, protons generally point downwards and possess energy of greater than 100 MeV.

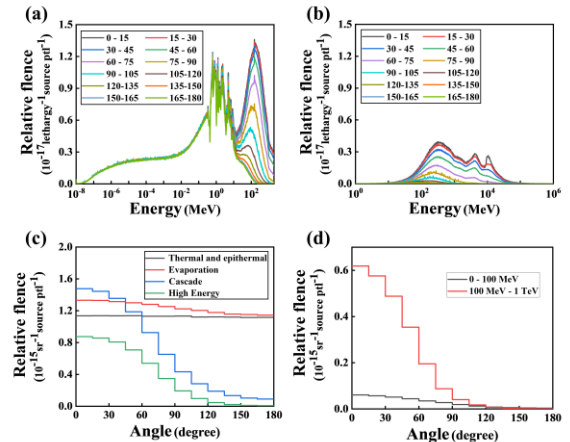


Figure 3. The energy spectra of (a) neutrons and (b) protons for various angle ranges and the angular distributions of (c) neutrons and (d) protons at 12.5 km altitude for various energy ranges.

3.2. Neutrons and protons passing through the ULD container

Fig. 4 shows the relative fluence of neutrons and protons passing through each side of the M-1 container. The simulation geometry, including that of the source, was modified, thus the data were normalized and adjusted to the new geometry. The numbers of particles that reach the four lateral surfaces are relatively homogenous, with a number difference of within 2% between surfaces; thus, the data from these surfaces were averaged for evaluation. The largest number of particles, both neutrons and protons, pass through the top of the container due to the nature of particle angular distribution; this trend is especially accentuated with high energy neutrons and protons. Furthermore, it should be noted that protons hardly pass through the bottom surface, therefore, to minimize the weight of the container while maintaining effective shielding,

reinforcement should be focused primarily on the top and lateral surfaces.

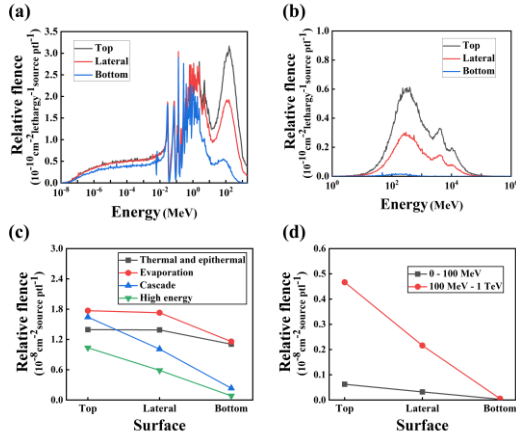


Figure 4. Energy spectra of (a) neutrons and (b) protons and relative fluence for various energy groups of (c) neutrons and (d) protons passing through a particular side of the container

3.3. Structural optimization

In this study, stainless steel (SS) and borated polyethylene (BPE) were selected as shielding material. The optimization was performed to find the dimensional conditions at which the number of neutrons and protons that reach the inner contents of the container is minimized. Some assumptions were introduced for the optimization calculation based on the results shown in the previous section. First, the thicknesses of BPE at the top and lateral surfaces were set to be equal due to the presence of low energy neutrons being nearly uniform at the top and lateral surfaces. Since the number of neutrons incident on the bottom is not nearly as large as that observed incident on the top or lateral surfaces, the BPE layer at the bottom does not need to be as thick as it is at other sides.

Fig. 5 shows the relative fluence of low energy neutrons that pass through the BPE layer as a function of ratio between the thickness of the layer at the top and that at the bottom while keeping the total weight of BPE fixed. The results indicate that the ratio value of between 0.8 and 1.5 provides good shielding against low energy neutrons.

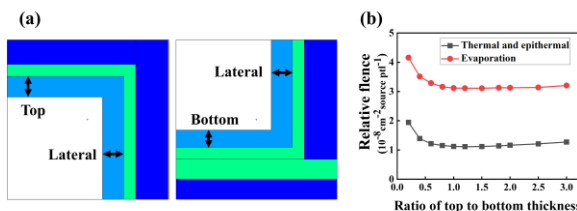


Figure 5. The geometry of the BPE layer. The relative fluence of neutrons in the (b) thermal, epithermal groups and evaporation group of neutrons after passing BPE

Likewise, a similar procedure was performed with SS to determine the optimal condition at which high energy neutrons and protons are most effectively shielded against. Since only a very few number of high energy neutrons and protons are incident on the bottom, the side will not be reinforced with SS. Fig. 6 shows the relative fluence of high energy neutrons and protons that pass through the SS layer as a function of ratio between the thickness of the layer at the top and that at the sides while keeping the total weight of the steel fixed. The results indicate that the ratio value of between 1.5 and 2.5 provides good shielding against high energy neutrons and protons.

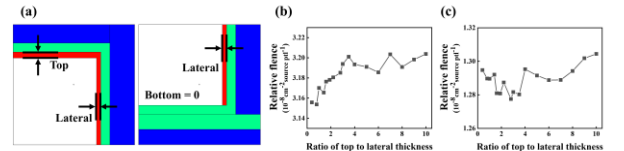


Figure 6. (a) The geometry of the SUS layer. The relative fluence of neutrons in the (b) high energy group of neutrons and the (c) protons (<1 TeV) after passing BPE

With the optimal ratios determined, calculations were performed to establish which of the two, BPE or SS, would be better used as the outer shielding material. Fig. 7 shows the two possible cases of structural arrangement: having SS placed inside the BPE, and vice versa. Generally, it is considered ideal to have high-Z material on the outside, however, due to the relatively high density of SS, having it on the outside would increase the weight of the complete system as more material is required for the outer layer than the inner layer. With the weight limit in place, this would imply that the thickness of the SS layer would have to be compromised. In comparison, when the SS is located on the inside, the neutrons attenuated by PE may generate secondary particles as it passes through the steel layer; however, the layer can be thicker. To quantitatively evaluate both cases, calculations were carried out by varying the thickness of PE and SS. As determined previously, PE was set to have the same thickness at all lateral surfaces, while the thickness of SS at the top surface doubled that at the lateral surfaces. Taking into account the weight limit of the M-1 container, the total weight limit for the shielding material was set to 5,000 kg. The weight of BPE and SS was varied in 500 kg intervals during the trials.

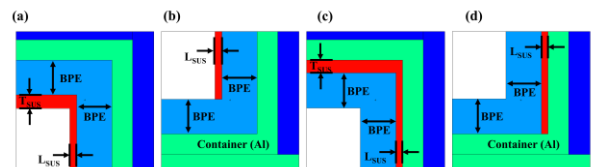


Figure 7. The cross section of (a) upper and (b) lower side for case 1 (SUS inside BPE) and (c) upper and (d) lower side for case 2 (BPE inside SUS).

Fig. 8 shows how the flux of neutrons and protons attenuates for different energy groups as the particles pass through the shielding material. Except against the neutrons in the evaporation group, superior shielding capability was observed in the case of having SS located inside BPE than in the case of vice versa. The above-mentioned exception arises from the fact that secondary neutrons generated by neutrons or protons interacting with high Z materials have energy corresponding to that of neutrons in the evaporation group. However, the difference in shielding capability against evaporation neutrons between the two cases was not significant enough to warrant having SS on the outside. Thus, from the results, it was concluded that it was most optimal to have SS located inside BPE with the weight of each material being between 2000 kg and 3000 kg for BPE and 3000 kg and 2000 kg for SS.

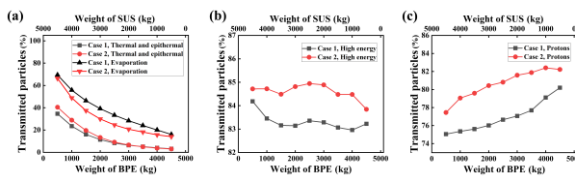


Figure 8. Percentage of transmitted (a) neutrons and (b) protons of various energy groups

3.4. Neutrons and protons at different position of containers inside air freighter

Fig. 10 represents the neutrons and protons at different position of containers inside aircraft when the air freighter was modeled, not just a simplified fuselage, but also wings, engines, and fuel tanks. For Fig. 10(a) and (b), the top three lines represent attenuated neutrons for each energy region, and the bottom three lines represent neutrons produced by protons. Similarly, for (c) and (d), the top three lines represent attenuated protons for each energy region, and the bottom three lines represent protons produced by neutrons. The neutrons and protons were reduced by 25% in the vicinity of the fuel tank. This is because of the high content of carbon and hydrogen in airplane fuel, which is similar to the effect of PE attenuating low energy neutrons and protons. However, assuming that the fuel tank is full, the attenuating effect is expected to be smaller than this.

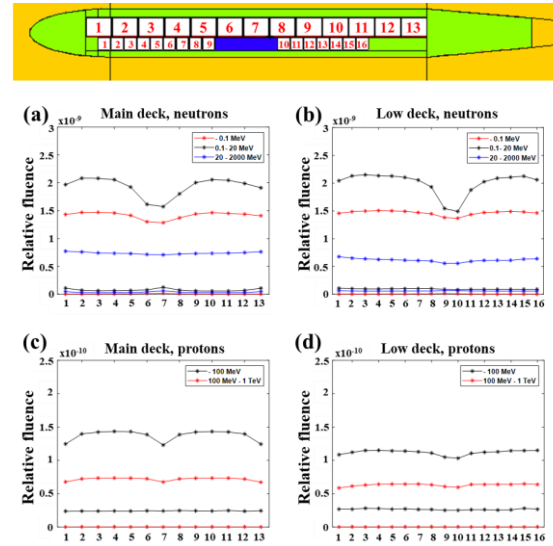


Figure 9. Neutrons at each containers on (a) main deck and (b) low deck, and protons at each containers on (a) main deck and (b) low deck

3. Conclusions

To reduce the possibility of unexpected failure of semiconductors packaged for air transport, the optimal conditions to shield against cosmic ray-induced particles were determined using Monte Carlo simulation. BPE and SS, when used together, proved to be effective at reducing the number of incoming neutrons and protons at the flight altitude, and thus, were adopted as the shielding materials. Also, when the radiation sensitive air cargos were located near the fuel tank, the probability of failure caused by neutrons or protons can be reduced.

REFERENCES

- [1] Pazianotto, M., et al., Extensive air shower Monte Carlo modeling at the ground and aircraft flight altitude in the South Atlantic Magnetic Anomaly and comparison with neutron measurements. Astroparticle Physics, 2017. 88: p. 17-29.
- [2] F. Pazianotto, M., et al., Analysis of the angular distribution of cosmic-ray-induced particles in the atmosphere based on Monte Carlo simulations including the influence of the Earth's magnetic field. Astroparticle Physics, 2018. 97: p. 106-117.
- [3] Normand, E. and T. Baker, Altitude and latitude variations in avionics SEU and atmospheric neutron flux. IEEE transactions on Nuclear Science, 1993. 40(6): p. 1484-1490.
- [4] Normand, E., Single-event effects in avionics. IEEE Transactions on nuclear science, 1996. 43(2): p. 461-474.
- [5] Boruzdina, A.B., et al., Microdose effects in SRAM cells under heavy ion irradiation. 2017 17th European Conference on Radiation and Its Effects on Components and Systems (Radecs), 2017: p. 482-484.
- [6] Haran, A., et al., Single Event Hard Errors in SRAM Under Heavy Ion Irradiation. Ieee Transactions on Nuclear Science, 2014. 61(5): p. 2702-2710.